Minimal Throughput Maximization of UAV-enabled Wireless Powered Communication Network in Cuboid Building Perimeter Scenario

Qiang Tang, Yong Yang, Lixin Liu, Kun Yang, *Fellow, IEEE,*

***Abstract*—As the number of Internet of Things Devices (IoTDs) increases, the building Structural Health Monitoring (SHM) system is subject to the enormous amount of data collected from sensors. To tackle this challenge, we investigate an Unmanned Aerial Vehicle (UAV)-enabled Wireless Powered Communication Network (WPCN) in a building SHM scenario where a UAV is dispatched to provide wireless charging and data relaying services for IoTDs on the building. For preventing the channel blockage caused by the building, we place the UAV and Access Points (APs) in specific trajectory and locations, respectively. To improve the system's throughput, we maximize the minimum data volume among devices in a given period by formulating an optimization problem in which we jointly optimize the link schedule, the power and time allocation and the hovering positions of the UAV. However, the formulated problem is a mixed-integer nonlinear programming and is hard to solve. Therefore, we adopt a bottleneck-aware idea to reduce the dimensionality of the optimization variables in order to obtain a simplified problem that can be solved in a low-complexity way. Also, the Block Coordinate Descent (BCD) method is applied to reduce the complexity of the problem. Meanwhile, we further propose a method to deal with the heterogeneous problem for improving the generalizability of our algorithm. To estimate the performance of our proposed algorithm, we compare it with the Monte Carlo (MC) method, Game Theory (GT) and Particle Swarm Optimization (PSO). The simulation results indicate that our algorithm can obtain better performance.**

***Index Terms*—Structural health monitoring, wireless powered communication network, unmanned aerial vehicle, bottleneck-awared.**

I. Introduction

Structural Health Monitoring (SHM) is extensively studied to estimate structural damage of buildings, aerospace vehicles, bridges, *etc.*, with the information provided by IoTDs/sensors about any significant change or damage occurring in a structure. In the building SHM area, the detection of structural damage is essential in ensuring structural safety during a building's lifetime [1].

For traditional wired system for building SHM, it is necessary to install the cables, and the IoTDs needs more maintenance. To solve this problem, Wireless Sensor Network (WSN) system is studied as data collecting system for SHM to replace traditional wired system. The IoTDs in the WSN transmit data through the wireless channel toward the Access Points (AP) equipped with the edge servers to facilitate data aggregation and processing.

However, IoTDs produce more data because of the advance of sensors such as the optical fiber sensor, pressure sensor, humidity and temperature sensors, which increases the communication burden. Moreover, the IoTDs usually have limited battery energy, which causes they can hardly process the data transmission for a long lifetime. For increasing IoTDs' lifetime, and for avoiding any maintenance, Wireless Power Transfer (WPT) can provide the devices with sustainable energy supply via Radio Frequency (RF) radiation to charge the battery of IoTDs [2]. By integrating WPT technology into WSN, a new architecture named Wireless Powered Communication Network (WPCN) has attracted substantial research interests [3]. In WPCN, the APs can broadcast RF energy signals to the IoTDs and receive their own data, and the IoTDs use the harvested energy to communicate with the APs.

Although WPT can provide sufficient energy, the long distance between the AP and the IoTDs results in low communication rate and energy transfer efficiency. Especially in the building SHM scenario, when the AP is located on the ground and part of the IoTDs are located on the top surface of the building, the Line-of-Sight (LoS) connection will be blocked by the building. Therefore, we utilize an Unmanned Aerial Vehicle (UAV) as Hybrid Relay Node (HRN) to broadcast RF energy to IoTDs and forward IoTDs' data to APs. UAV has attracted substantial research interests in the field of communications due to its high flexibility, mobility, low cost and strong LoS channels with IoTDs [4], [5]. UAV-enabled WPCN can achieve ubiquitous coverage, establish strong communication links, as well as improve the energy efficiency of WPT.

In this paper, as shown in Fig. 1, we consider a UAV-enabled WPCN in a building SHM scenario where the IoTDs are located at the surfaces of a cuboid-shaped building, including the top plane. The APs, *e.g. electric vehicles*, with edge servers are deployed at the ground to collect and process data from the IoTDs via wireless channels. To tackle the problem that the devices on the top plane cannot link directly with the APs, we utilize a UAV to forward data from the IoTDs to the APs, as well as to charge the IoTDs to prolong the work period. By using high power forwarding services of the UAV, the system can obtain higher data transmission rate and lower energy consumption of IoTDs. Specifically, in order to ensure the lowest communication capacity of the system, our goal is

Qiang Tang, Yong Yang and Lixin Liu are with the School of Computer Science & Communication Engineering, Changsha University of Science & Technology, Changsha, Hunan, 410114, China. (emails: tangqiang@csust.edu.cn; 21208051635@stu.csust.edu.cn; 20208051436@stu.csust.edu.cn)

Kun Yang is with the School of Computer Science and Electronic Engineering, University of Essex, Essex CO4 3SQ, U.K. (email: kunyang@essex.ac.uk)

Corresponding author: Kun Yang.

to maximize the minimal throughput among all devices with consideration of the energy harvesting constraints.

The main contributions of this paper are:

1) A new application scenario of the UAV-enabled WPCN is proposed where a UAV is dispatched to charge and collect data from the IoTDs on the surface of a cuboid building in the building SHM scenario. To prevent the communication from being blocked by the building, we ensure the LoS communication channel by reasonably arranging the UAV and APs. Considering the amount of IoTDs is quite large, we maximize the minimal throughput among IoTDs by jointly optimizing the link schedule, UAV hovering positions and wireless resource allocation. Besides, the proposed scenarios can be used not only in the building SHM situation, but also in situations with similar physical structures such as construction site surveillance, building fire rescue, and edge computing in stadium.

2) In order to efficiently tackle the formulated mixed integer nonlinear programming (MINLP) problem, we propose a bottleneck-awared heuristic alternating algorithm. We reduce the dimensionality of the variables by finding the bottleneck in the system to obtain a simplified problem that can be solved in a very low-complexity way. Also, the Block Coordinate Descent (BCD) method is applied to reduce the complexity of the problem.

3) Our proposed algorithm can only cope with the case where all IoTDs are homogeneous (*i.e.* all IoTDs have similar rate requirements). To improving the generalizability of our algorithm, we further propose a method to deal with the heterogeneous IoTDs problem. First, we define a baseline rate requirement γ. For the IoTDs have different rate requirements, we can assume their requirements to be integer multiples of γ. Then, if an IoTD's requirement is $x\gamma$, we treat it as x homogeneous virtual IoTDs in the same location. The problem consisting of all virtual IoTDs is homogeneous, which can be solved by our proposed algorithm.

4) We compare our proposed algorithm with benchmark algorithms that include the GT, MC method over some system parameters. The results show that our algorithm can achieve a better solution within a much shorter time. We also evaluate the performance of part of our algorithm which optimizes the UAV's hovering point by comparing with the PSO and MC methods. It comes out that our algorithm can take less time to achieve the same optimal value.

II. Related Work

A. Building Structural Health Monitoring

Building SHM is an automated system of monitoring variations in the geometric and material qualities of buildings, and helps to predict the damage of the structure. Sensors used in SHM are designed to measure strain, stress, vibration, tilt, humidity, and temperature of current state of the structure.

Im *et al.* [6] designed a smart structural-durability health-monitoring system where each IoTD is composed of multisensing sensors, a 900-MHz wideband antenna and a data communication module that supports IEEE standard 802.15.4. The data acquired by sensors is sent to the gateway and remote user's software via the antenna. This system can detect the durability condition at an early stage of concrete deterioration. Misra *et al.* [7] studied a wireless module that can generate and detect highly nonlinear solitary waves for SHM scenarios. In this module, a sensor is in contact with the material, and is wired to the data acquisition system for storing the time series for post-processing. The communication in this module is implemented by the Bluetooth module that is suitable for short and midrange distance communication and does not need any external network. Yan *et al.* [8] analyzed the problems of untimely and inaccurate sensor fault diagnosis in the building SHM system, and optimize the communication load and energy efficiency for massive IoTDs. Meanwhile, a sensor fault self diagnosis method is proposed.

B. UAV-enabled WPCN System

Depending on the objective, different problems have been considered to improve the performance of UAV-enabled WPCN in the existing literature.

Energy related optimization became the common research problem in UAV-enabled WPCN, which aims to make the system working longer in an energy-stressed situation and save energy cost [9]–[13]. Beak *et al.* [9] integrated a UAV in wireless charging sensor networks. Their objective was to maximize the minimum energy of sensors after data transmission and energy harvesting under data collection and UAV energy constraints. They jointly optimize the UAV hovering position and time by Lagrange multiplier method and their proposed geometry-based algorithm. Hu *et al.* [10] expected a UAV-enabled wireless powered MEC architecture, and a problem was formulated to minimize the long-term average energy efficiency with considering of the stochastic task arrivals and random channel conditions The authors proposed a low-complexity online computation offloading and trajectory scheduling algorithm to optimize the system resources and the UAV's trajectory. Gu *et al.* [11] proposed a security awared UAV-MEC scheme where energy harvesting is studied and the eavesdropper is considered. The energy consumption for UAV was minimized by optimizing the computation and communication resource allocation with considering of the computation-latency constraint. To solve the nonconvex problem, the authors convert it into a convex one by analytical means.

Communication capacity maximization has also been studied recently [14]–[19]. Xie *et al.* [14] studied a UAV-assisted WPCN, in which a UAV is dispatched as the WPT charger and the mobile AP to serve the territorial users. The authors maximized the uplink minimal throughput by solving a problem which is subject to the UAV's maximum speed constraint and the users' energy harvesting constraints. Meanwhile, the trajectory of UAV and the resource allocation are optimized in the problem. To solve the formulated problem, the authors obtain the locally optimal solution by alternating optimization and successive convex programming. Xie *et al.* [15] considered a WPCN scenario which contains two UAVs and two users. And the co-channel interference for wireless information transfer is mitigated. In order to minimize the

uplink minimum throughput of the users, a problem was formulated to optimize the two UAVs' trajectories and the communication resources allocation subject to the maximum speed and collision avoidance constraints of UAVs, as well as the energy harvesting constraints of devices. The problem is solved by alternating optimization and successive convex approximation. Du *et al.* [16] discussed a non-orthogonal multiple access system where a UAV is deployed to perform WPT service, and a problem aiming to maximize the sum rate of the system is taken into account.

For the delay minimization area, the service latency is minimized to perform the delay-sensitive tasks [20], [21]. Wang *et al.* [20] combined the task offloading decisions optimization, connection scheduling and resource allocation to minimize the service latency of all users in the proposed UAV-assisted wireless powered MEC Beyond 5G network. Wang *et al.* [21] minimized the time required by a UAV in the UAV-assisted WIT and WPT system via jointly optimizing the trajectory of the UAV and the transmission scheduling of all users.

It is important to ensure that the IoT systems work robustly in some application scenarios, where the packet loss rate is considered [22], [23]. Ponnimbaduge Perera *et al.* [22] studied a UAV aided wireless powered sensor network where a UAV collects data form the cluster headers of sensor nodes, and the sensor nodes harvest energy from the power beacons via RF-WPT. The authors formulated a problem to minimize the outage probability of the system by optimizing resource allocation. Li *et al.* [23] investigated the resource management problem to minimize the overall data packet loss of the IoTDs in their proposed UAV-assisted wireless powered IoT scenario with a deep Q-learning method.

The papers above assume that devices are located in a flat plane, and the UAV's feasible position falls within the free 2D plane or 3D space. However, in the building SHM scenario, IoTDs are in the vicinity of the building. The blockage caused by the building may effect the communication channels between the UAV and the IoTDs installed on the surface of the building. In this paper, we take a UAV-enabled WPCN application scenario, the building SHM scenario, into consideration. To overcome the blockage and meanwhile simplify the formulated problem, we design the trajectory of the UAV and the positions of the ground APs in an reasonable manner. The UAV performs a hover-and-fly working method, and the hovering locations are optimized in our problem.

Moreover, we innovatively propose a bottleneck-aware algorithm combined with Lagrange and BCD methods, which can effectively reduce the complexity of the algorithm and improve the efficiency of the solution. This approach divides a problem that requires consideration of multiple IoTDs into two steps to solve, with the first step trying to identify the bottleneck IoTD and then solving a simplified problem that includes only the bottleneck IoTD.

The rest of this paper is organized as follows. Section III describes the system model. In section IV, the optimization problem is formulated, and our proposed algorithm is described. The numerical analysis is performed in section V. In the last section, we give the conclusion of this paper.

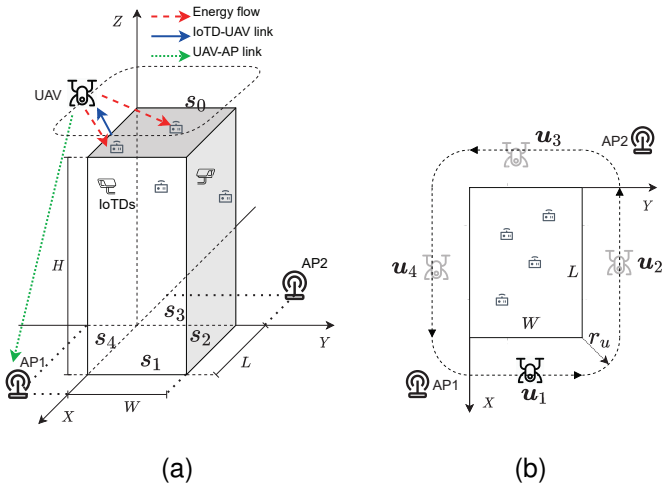

Fig. 1. (a) The UAV-enabled WPCN. (b) The trajectory of the UAV.

TABLE I
LIST OF SYMBOLS

Parameter	Meaning
L, W, H	length, width, height of building
I	set of indices of four hovering points
s_i	the i-th plane
n_i	number of the IoTDs in the plane s_i
N_i	set of IoTDs in the plane s_i
N	number of all IoTDs
$\boldsymbol{\omega}_{i,k}$	coordinate of the k-th IoTD in the plane s_i
$\boldsymbol{\omega}_{ap}^{i}$	coordinate of the i-th AP
H_u	UAV's safety height above the building
$\boldsymbol{u}_i$	coordinate of the i-th hovering point
r_u	UAV's horizontal safety distance
v	UAV's flying velocity
T	working period of the UAV
T^{fly}	flying time of the UAV within one period
η	WPT energy conversion efficiency

III. SYSTEM MODEL

As shown in Fig. 1(a), we assume a cuboid building whose five flat surfaces are deployed with IoTDs. Specifically, the top surface is denoted as s_0, and the four side surfaces are denoted as $s_i, \forall i \in I = \{1, 2, 3, 4\}$. We consider a UAV-aided WPCN that includes one rotary-wing UAV, two APs and N IoTDs. The number of IoTDs on s_i is $n_i, \forall i \in \{0\} \cup I$, and the total amount of IoTDs is $N = \sum_{i \in \{0\} \cup I} n_i$. We denote the set of the IoTDs on plane s_i by $N_i = \{1, 2, \ldots, n_i\}, \forall i \in I \cup \{0\}$. The main symbols in this paper are summarized in TABLE I.

In our model, IoTDs generate an amount of computing tasks which need to be offloaded to the edge servers on the ground APs with the forwarding of the UAV. The UAV is utilized as a mobile relay to help this information exchange. Furthermore, the UAV is equipped with a RF charger and plays a role as a mobile energy transmitter to wirelessly charge those low-power IoTDs on the building. On the ground, the two APs are equipped with ultra-high-performance CPUs and they are capable of fast calculation.

A. Geometric Model

Without loss of generality, we consider a 3D Euclidean coordinate system as illustrated in Fig. 1(a). This building has a height H, a width W and a length L. IoTDs

are randomly distributed on the building's surfaces. We use $\boldsymbol{w}_{i,k} = (x_{i,k}, y_{i,k}, z_{i,k})$ to notate the position of k-th IoTD on the plane s_i. In order to avoid the shadowing fading caused by the building and meanwhile save cost, two APs are deployed at $\boldsymbol{w}_1^{ap} = (x_1^{ap}, y_1^{ap}, 0)$ and $\boldsymbol{w}_2^{ap} = (x_2^{ap}, y_2^{ap}, 0)$, which are near the two opposite corners of the building. The UAV flies at a fixed altitude $H + H_u$ and connects with IoTDs only at the four hovering positions named $\boldsymbol{u}_i = (x_i, y_i, H + H_u), \forall i$, where H_u means the safety height above the building.

For the sake of security and better access channel between UAV and APs, the UAV's horizontal trajectory is shown in Fig. 1(b) with a fixed radius r_u which symbolizes the horizontal safety distance. The four hovering points $\boldsymbol{u}_i$ fall on the four straight lines of the trajectory, which can guarantee a LoS communication channel between the UAV and the IoTDs. The optimizable part of the $\boldsymbol{u}_i$ are $\boldsymbol{U} = \{y_1, x_2, y_3, x_4\}$. For ease of illustration, we define u_i as the alias of the element in $\boldsymbol{U}$, where

$$u_1 \triangleq y_1, u_2 \triangleq x_2, u_3 \triangleq y_3, u_4 \triangleq x_4.$$

Therefore, the $\boldsymbol{U}$ can be rewritten as $\boldsymbol{U} = \{u_i, \forall i\}$, and the geometric constraints about the hovering points is

$$0 \le u_i \le u_i^{max}, \quad \forall i \in I \tag{1}$$

where $u_1^{max} = u_3^{max} = W, u_2^{max} = u_4^{max} = L$.

B. Link Schedule

At $\boldsymbol{u}_i$, the UAV connects to IoTDs in the set N_i and a portion of IoTDs in set N_0 for performing relaying and charging service. We introduce a $4 \times n_0$ dimensional matrix $\boldsymbol{\alpha} \triangleq (\alpha_{i,j})_{4\times n_0}$ to express the link schedule between the top IoTDs and the UAV hovering position, and $\alpha_{i,j} = 1$ means they are connected, otherwise $\alpha_{i,j} = 0$. In our model, the UAV can serve at most C IoTDs at a hovering point simultaneously. Hence, it yields the following constraints about the link schedule $\boldsymbol{\alpha}$:

$$\alpha_{i,j} \in \{0, 1\}, \quad \forall j \in N_0, \forall i \in I, \tag{2}$$

$$\sum_{i\in I} \alpha_{i,j} = 1, \quad \forall j \in N_0, \tag{3}$$

$$\sum_{j\in N_0} \alpha_{i,j} \le C - n_i, \quad \forall i \in I. \tag{4}$$

After introducing the $\boldsymbol{\alpha}$, we represent the set of IoTDs which are linked to $\boldsymbol{u}_i$ as

$$N_i^c = \{1, 2, \ldots, n_i + c_i\}, \quad \forall i \in I, \tag{5}$$

where $c_i = \sum_{j\in N_0} \alpha_{i,j}$ is the number of the top IoTDs which are linked to $\boldsymbol{u}_i$. Meanwhile, the alias of the location of the k-th IoTD in N_i^c is $\boldsymbol{w}_{i,k}^c$.

As for the connection between UAV and the APs, the UAV communicates with $\boldsymbol{w}_1^{ap}$ when it is hovering at $\boldsymbol{u}_1, \boldsymbol{u}_4$, and establishes a connection with $\boldsymbol{w}_2^{ap}$ at $\boldsymbol{u}_2, \boldsymbol{u}_3$.

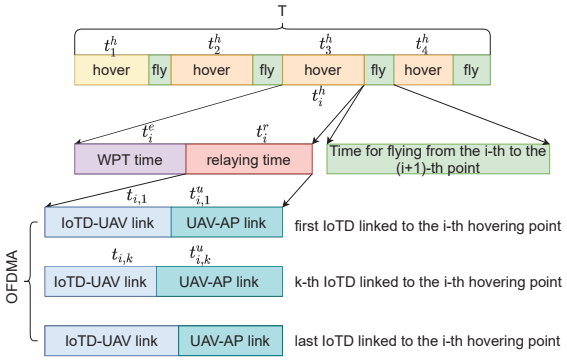

Fig. 2. System working time allocation.

C. Time Division

The working duration is cyclical. During each period T, the UAV starts at $\boldsymbol{u}_1$ and takes a flight around the fixed trajectory with a linear constant acceleration a and a maximum velocity v in a successive hover-and-fly manner [25], [26]. Moreover, we assume that the UAV undergoes three phases during each segment of flight: acceleration, constant speed and deceleration. Therefore, the total flight time is

$$T^{fly} = \frac{2\pi r_u + 2(W + L)}{v} + \frac{4v}{a}. \tag{6}$$

Fig. 2 shows the UAV's working time allocation structure in our system. At $\boldsymbol{u}_i$, it takes the UAV t_i^h seconds to hover and work. The constraint about the UAV's hovering time is

$$\sum_{i\in I} t_i^h \le T - T^{fly}. \tag{7}$$

The hovering time t_i^h is further divided into two phases: the relaying phase and the WPT phase, which occupy t_i^r and t_i^e, respectively. Therefore, we have

$$t_i^r + t_i^e \le t_i^h, \quad \forall i \in I. \tag{8}$$

1) Relaying Phase: During the relaying phase, the UAV is dispatched to relay data from IoTDs to the related AP. It can be assumed that the wireless channel between the UAV and each IoTD is dominated by LoS due to the pre-designed UAV trajectory. Thus, we can get the channel power gain between $\boldsymbol{u}_i$ and $\boldsymbol{w}_{i,k}^c$, which is denoted by $h_{i,k}^c$, as

$$h_{i,k}^c = \frac{h_0}{(d_{i,k}^c)^2}, \quad \forall k \in N_i^c, \forall i \in I, \tag{9}$$

where h_0 is the channel power gain at a reference distance $d_0 = 1$ m and $d_{i,k}^c = \|\boldsymbol{w}_{i,k}^c - \boldsymbol{u}_i\|_2$.

As for the UAV-AP channel, the power gain h_i^u is

$$h_i^u = \frac{h_0}{(d_i^u)^2}, \quad \forall i \in I, \tag{10}$$

where $d_1^u = \|\boldsymbol{w}_1^{ap} - \boldsymbol{u}_1\|_2, d_2^u = \|\boldsymbol{w}_2^{ap} - \boldsymbol{u}_2\|_2, d_3^u = \|\boldsymbol{w}_2^{ap} - \boldsymbol{u}_3\|_2, d_4^u = \|\boldsymbol{w}_1^{ap} - \boldsymbol{u}_4\|_2$.

The Orthogonal Frequency Division Multiple Access (OFDMA) scheme is considered to mitigate the channel interference among IoTDs. We divide the frequency bandwidth

into C orthogonal subchannels. Therefore, we can get communication rates $R^c_{i,k}$ and $R^u_{i,k}$ which represent the rate from $\boldsymbol{w}^c_{i,k}$ to $\boldsymbol{u}_i$ and the rate from $\boldsymbol{u}_i$ to its related AP, respectively, as

$$R^c_{i,k} = \frac{B}{C}\log_2(1+\frac{p^c_{i,k}h^c_{i,k}}{N_0}), \quad \forall k \in N^c_i, \forall i \in I, \tag{11}$$

$$R^u_i = \frac{B}{C}\log_2(1+\frac{p^u_i h^u_i}{N_0}), \quad \forall i \in I, \tag{12}$$

where N_0 denotes the noise power, B is the whole transmission bandwidth, $p^c_{i,k}$ is the transmit power of the k-th IoTD in N^c_i, and p^u_i is the transmission power of the UAV at $\boldsymbol{u}_i$.

At $\boldsymbol{u}_i$, the relaying time t^r_i is composed of two parts: the IoTD-UAV offloading time and the UAV-AP transmission time for each IoTD. We use $t^c_{i,k}$ to represent the IoTD-UAV task offloading time from IoTD $\boldsymbol{w}^c_{i,k}$ to the UAV. The variable $t^{uc}_{i,k}$ is used to be the symbol of the time for the UAV to transmit the data from IoTD $\boldsymbol{w}^c_{i,k}$ to the related AP. We get the time constraint in the relaying phase:

$$t^c_{i,k} + t^{uc}_{i,k} \le t^r_i, \quad \forall k \in N^c_i, \forall i \in I. \tag{13}$$

2) WPT Phase: At $\boldsymbol{u}_i$, we assume the RF energy transmit power as p^e_i, and the IoTDs' harvested energy during the WPT time t^e_i are:

$$\hat{E}^c_{i,k} = \eta h^c_{i,k} p^e_i t^e_i, \quad \forall k \in N^c_i, \forall i \in I, \tag{14}$$

where $\eta \in (0,1)$ is the energy conversion efficiency.

The energy consumption of each IoTD is:

$$E^c_{i,k} = p^c_{i,k} t^c_{i,k}, \quad \forall k \in N^c_i, \forall i \in I. \tag{15}$$

To ensure that the energy captured by the IoTD through the WPT meets its communication requirements, we have the energy harvesting constraint:

$$E^c_{i,k} - \hat{E}^c_{i,k} \le 0, \quad \forall k \in N^c_i, \forall i \in I. \tag{16}$$

IV. Problem Formulation and Algorithm Design

A. Problem Formulation

In this paper, our purpose is to improve data throughput in the network with aware of fairness among all IoTDs. Therefore, the objective is to maximize the minimal data throughput among all IoTDs, which is equivalent to maximize the minimal transmitted data volume among IoTDs in a given working period T. In our model, we maximize the objective by optimizing the IoTD's transmit power $\boldsymbol{p}^c \triangleq \{p^c_{i,k}\}$, link schedule $\boldsymbol{\alpha}$, hovering positions $\boldsymbol{U}$, IoTD's communication time $\boldsymbol{t}^c \triangleq \{t^c_{i,k}\}$, UAV's forwarding time $\boldsymbol{t}^{uc} \triangleq \{t^{uc}_{i,k}\}$, UAV's communication time $\boldsymbol{t}^r \triangleq \{t^r_i\}$, UAV's WPT time $\boldsymbol{t}^e \triangleq \{t^e_i\}$, hovering time $\boldsymbol{t}^h \triangleq \{t^h_i\}$. For convenience, we define the set of all time variables as $\boldsymbol{t} \triangleq \{\boldsymbol{t}^c, \boldsymbol{t}^{uc}, \boldsymbol{t}^r, \boldsymbol{t}^e, \boldsymbol{t}^h\}$.

The problem can be formulated as **P1**:

$$(\mathbf{P1}): \max_{\boldsymbol{p}^c, \boldsymbol{\alpha}, \boldsymbol{U}, D, \boldsymbol{t}} \quad D \tag{17}$$

$$s.t. \quad D - t^c_{i,k}R^c_{i,k} \le 0, \qquad \forall k \in N^c_i, \forall i \in I, \tag{17a}$$

$$D - t^{uc}_{i,k}R^u_i \le 0, \qquad \forall k \in N^c_i, \forall i \in I, \tag{17b}$$

$$E^c_{i,k} - \hat{E}^c_{i,k} \le 0, \qquad \forall k \in N^c_i, \forall i \in I, \tag{17c}$$

$$\sum_{i \in I} t^h_i \le T - T^{fly}, \tag{17d}$$

$$t^r_i + t^e_i \le t^h_i, \qquad \forall i \in I, \tag{17e}$$

$$t^c_{i,k} + t^{uc}_{i,k} \le t^r_i, \qquad \forall k \in N^c_i, \forall i \in I, \tag{17f}$$

$$\alpha_{i,j} \in \{0,1\}, \qquad \forall j \in N_0, \forall i \in I, \tag{17g}$$

$$\sum_{i \in I} \alpha_{i,j} = 1, \qquad \forall j \in N_0, \tag{17h}$$

$$\sum_{j \in N_0} \alpha_{i,j} \le C - n_i, \qquad \forall i \in I, \tag{17i}$$

$$0 \le u_i \le u^{max}_i, \qquad \forall i \in I, \tag{17j}$$

where D is an auxiliary variable representing the minimal data volume which can be ensured from constraints (17a) and (17b).

(17a) and (17b) guarantee that D is less than the data volume of all IoTDs. (17c) is the energy harvesting causality constraint. (17d) indicates the maximum constraint of the sum of hovering time at each hovering point. (17e) means that the sum of charging time and data relaying time is less than the hover time. (17f) indicates that the forwarding time is less than the sum of the IoTD-UAV and the UAV-AP communication time for each IoTD. (17g)-(17i) are the constraints *w.r.t.* the link schedule. (17j) is the upper and lower bound constraint of hovering position.

P1 is nonconvex due to (17a)-(17c). The reason is that $z = xf(y)$ is nonconvex *w.r.t.* x and y for the determinant of the Hessian matrix of z, (*i.e.* $-(f'(y))^2$) is less than zero.

P1 is a non-convex MINLP problem which generally cannot be solved in polynomial time. In order to solve the problem efficiently, we proposed an iterative algorithm based on the BCD method to obtain a sub-optimal solution.

B. Link Schedule Optimization

When the $\boldsymbol{p}^c, \boldsymbol{U}, \boldsymbol{t}$ is given, the problem **P1** becomes a sub-problem where only the $\boldsymbol{\alpha}$ and D are optimizable. We proposed a heuristic algorithm to acquire a sub-optimal solution of the sub-problem.

Note that our goal is to maximize the minimal data volume among all IoTDs, so it is easy to observe that the bottleneck IoTD which has the lowest power gain is more likely to limit the increase in the data volume. Then, in our algorithm, the bottleneck IoTD is give priority to establish a connection with its nearest hovering position. The proposed heuristic method is specified in **Algorithm 1**.

C. Power and Time Optimization

With fixed $\boldsymbol{U}$ and $\boldsymbol{\alpha}$, problem **P1** can be rewritten into **P2**:

$$(\mathbf{P2}): \max_{\boldsymbol{p}^c, D, \boldsymbol{t}} \quad D \tag{18}$$

$$s.t. \quad (17a) - (17f),$$

Algorithm 1 Link Schedule Optimizing

Input: $\boldsymbol{U}$;
Output: $\boldsymbol{\alpha}$;
Initialize $\boldsymbol{\alpha}$ with $\alpha_{i,j} \leftarrow 0$, $\boldsymbol{d}$ with $\boldsymbol{d}(i,j) \leftarrow \|\boldsymbol{w}_{0,j} - \boldsymbol{u}_i\|_2$, $\boldsymbol{ept}$ with $\boldsymbol{ept}(i) \leftarrow C - n_i$;
$\boldsymbol{d}(i,:) \leftarrow +\infty$ if $\boldsymbol{ept}(i) == 0, \forall i$.
while $\sum_i \boldsymbol{\alpha}(i,j) == 0, \exists j$ **do**
  Initialize two n_0-D arrays $\boldsymbol{compare}$ and $\boldsymbol{nearest}$;
  for $j \in N_0$ **do**
    if $\boldsymbol{\alpha}(i,j) == 1, \exists i$ **then**
      $\boldsymbol{compare}(j) \leftarrow 0$;
    else
      $\boldsymbol{compare}(j) \leftarrow \min_i \boldsymbol{d}(i,j)$;
      $\boldsymbol{nearest}(j) \leftarrow \arg\min_i \boldsymbol{d}(i,j)$;
    end if
  end for
  $ind \leftarrow \arg\max_j \boldsymbol{compare}$;
  $hov \leftarrow \boldsymbol{nearest}(ind)$;
  $\boldsymbol{\alpha}(hov, ind) \leftarrow 1$;
  $\boldsymbol{ept}(hov) \leftarrow \boldsymbol{ept}(hov) - 1$;
  $\boldsymbol{d}(hov,:) \leftarrow +\infty$ if $\boldsymbol{ept}(hov) == 0$.
end while
return $\boldsymbol{\alpha}$;

which is still non-convex.

1) Bottleneck-awared Problem Reduction: Suppose the optimal solutions of problem **P2** are $\{\boldsymbol{p}^{c*}, \boldsymbol{t}^*\}$ and the optimal value of the problem is D^*. In this case, from the (17a) and (17b), we get the optimal data volume of the k-th IoTD in the set N_i^c by

$$D_{i,k}^* = \min\{t_{i,k}^{c*} R_{i,k}^{c*}, \quad t_{i,k}^{uc*} R_i^u\}, \quad \forall k, \forall i, \tag{19}$$

where $R_{i,k}^{c*}$ is the $R_{i,k}^c$ with the optimal $\boldsymbol{p}^{c*}$. Similarly, we use D_i^* to indicate the optimized data volume among IoTDs in the set N_i^c. Thus, the definition of D_i^* is

$$D_i^* = \min_{k \in N_i^c} D_{i,k}^*, \quad \forall i \in I. \tag{20}$$

According to (17a), (17b), (19) and (20), the optimal value D^* should have

$$D^* = \min_{i \in I} D_i^*. \tag{21}$$

Lemma 1. $D_1^* = D_2^* = D_3^* = D_4^*$.

Proof. Without loss of generality, we assume that $D_1^* \le D_2^* \le D_3^* \le D_4^*$ and $D_1^* < D_4^*$. We firstly consider the case where $D_1^* < D_2^*$. To prove the assumption is false, we only need to construct a feasible solutions to reach a greater data volume than the optimal D^* obtained by $\{\boldsymbol{p}^{c*}, \boldsymbol{t}^*\}$. Note that when the $\boldsymbol{p}^c$ is given by $\boldsymbol{p}^{c*}$, the D_i^* is linear with the time variables $\boldsymbol{t}$. Thus, we construct a feasible solution by amplifying the value of $t_{1,k}^{c*}, t_{1,k}^{uc*}, t_1^{e*}, t_1^{r*}, t_1^{h*}$ to their $(1+\epsilon)$ times, where $\epsilon > 0$, as well as reducing the time distributed to the fourth hovering point. We define $\boldsymbol{D}_i^f$ as the minimal data volume that obtained by the newly constructed feasible solution. The ϵ is small enough to guarantee: the D_1^f is still the lowest among D_i^f. The objective value under the constructed solution is $D^f = D_1^f = (1+\epsilon) D_1^* > D_1^* = D^*$, which is contradictory with that the D^* is the optimal value. Therefore, in this case the assumption is false. In other cases when $D_1^* = D_2^*$ or $D_1^* = D_2^* = D_3^*$, the assumption can be similarly proved to be false, which proves **Lemma 1**. ■

According to **Lemma 1** and (21), we can get

$$D^* = D_i^*, \quad \forall i \in I. \tag{22}$$

Motivated by the previous heuristic **Algorithm 1**, the minimal data volume is mainly susceptible to the IoTDs which have the worse channel power gain. Thus, we define the Bottleneck IoTD (BIoTD) as the IoTD which has the worst channel power gain that linked to the same hovering position $\boldsymbol{u}_i, \forall i \in I$. According to the definition, there are four BIoTDs in our model. The index of the BIoTD in N_i^c is denoted by

$$b_i \in N_i^c, \quad \forall i \in I. \tag{23}$$

Correspondingly, the channel power gain between the BIoTD b_i and the $\boldsymbol{u}_i$ is denoted as h_i^{cb} which has

$$h_i^{cb} = \min_{k \in N_i^c} h_{i,k}^c, \quad \forall i \in I. \tag{24}$$

Supposing $\{p_i^{cb*}, t_i^{cb*}, t_i^{ucb*}\}$ to be the optimal values of the BIoTD b_i in $\{\boldsymbol{p}^{c*}, \boldsymbol{t}^*\}$ where $p_i^{cb*} = p_{i,b_i}^{c*}, t_i^{cb*} = t_{i,b_i}^{c*}, t_i^{ucb*} = t_{i,b_i}^{uc*}$, the optimal data volume of the BIoTD b_i is

$$D_i^{b*} = D_{i,b_i}^* = \min\{t_i^{cb*} \frac{B}{C} \log_2(1 + \frac{p_i^{cb*} h_i^{cb}}{N_0}), \quad t_i^{ucb*} R_i^u\}. \tag{25}$$

Lemma 2. $D_i^{b*} = \min_{k \in N_i^c} D_{i,k}^*, \quad \forall i \in I.$

Proof. Without loss of generality, we focus on one specified hovering point $\boldsymbol{u}_i$. We assume there exists an IoTD at $\boldsymbol{w}_{i,m}^c$ with $m \neq b_i$ and $D_{i,m}^* < D_i^{b*}$. In order to prove that the assumption is false, we construct a feasible solution by using the optimal power and time values of the BIoTD b_i to replace the corresponding values of the m-th IoTD in N_i^c. The newly achieved data volume by the m-th IoTD is $D_{i,m}^f > D_i^{b*} > D_i^{bf}$, which is conflict with the assumption. Then, the **Lemma 2** is proved. ■

According to (20)-(21) and **Lemma 2**, we can conclude that

$$D^* = D_i^{b*}, \quad \forall i \in I, \tag{26}$$

which means the minimal data volume of the system is only subject to the four BIoTDs. Only the BIoTDs are considered, we ignore the variables $\boldsymbol{p}^c, \boldsymbol{t}^c, \boldsymbol{t}^{uc}$ about the other IoTDs, and the problem **P2** is simplified to **P3**:

$$(\mathbf{P3}): \min_{\boldsymbol{p}^{cb}, D, \boldsymbol{t}^b} \quad -D \tag{27}$$

$$s.t. \quad D - t_i^{cb} \frac{B}{C} \log_2(1 + \frac{p_i^{cb} h_i^{cb}}{N_0}) \le 0, \quad \forall i \in I, \tag{27a}$$

$$D - t_i^{ucb} R_i^u \le 0, \quad \forall i \in I, \tag{27b}$$

$$p_i^{cb} t_i^{cb} - \eta h_i^{cb} p_i^e t_i^e \le 0, \quad \forall i \in I, \tag{27c}$$

$$\sum_{i \in I} t_i^h \le T - T^{fly}, \tag{27d}$$

$$t_i^r + t_i^e \le t_i^h, \quad \forall i \in I, \tag{27e}$$

$$t_i^{cb} + t_i^{ucb} \le t_i^r, \quad \forall i \in I, \tag{27f}$$

where $\boldsymbol{p}^{cb} = \{p_i^{cb}\}$ is the transmit power of the BIoTDs, $\boldsymbol{t}^{cb} = \{t_i^{cb}\}$ and $\boldsymbol{t}^{ucb} = \{t_i^{ucb}\}$ are the IoTD-UAV and the UAV-AP communication time vectors, respectively, and $\boldsymbol{t}^b \triangleq \{\boldsymbol{t}^{cb}, \boldsymbol{t}^{ucb}, \boldsymbol{t}^r, \boldsymbol{t}^e, \boldsymbol{t}^h\}$. The objective of the problem **P3** is to minimize $-D$, which is equivalent to maximize D.

It can be proved that if we use the optimal value $\boldsymbol{p}^{cb*}, \boldsymbol{t}^{cb*}, \boldsymbol{t}^{ucb*}$ of **P3** to replace the $\boldsymbol{p}^c, \boldsymbol{t}^c, \boldsymbol{t}^{uc}$ in **P2** and use the optimal $\boldsymbol{t}^{e*}, \boldsymbol{t}^{r*}, \boldsymbol{t}^{h*}, D^*$ in **P3** to replace the $\boldsymbol{t}^e, \boldsymbol{t}^r, \boldsymbol{t}^h, D$ in **P2**, the constraints of **P2** are still satisfied. Therefore, the optimal value of **P3** is achievable for **P2**.

2) Solve P3: In order to solve the problem **P3**, we denote $\boldsymbol{\lambda} = \{\lambda_i, \forall i\}$, $\boldsymbol{\lambda}^u = \{\lambda_i^u, \forall i\}$, $\boldsymbol{\lambda}^e = \{\lambda_i^e, \forall i\}$, μ, $\boldsymbol{\mu}^h = \{\mu_i^h, \forall i\}$ and $\boldsymbol{\mu}^r = \{\mu_i^r, \forall i\}$ to be the Lagrange multiplier vectors associated with the constraints (27a)-(27f), respectively [27]. Thus, the Lagrange function of **P3** is

$$\begin{aligned} &L(D, \boldsymbol{p}^{cb}, \boldsymbol{t}^b, \boldsymbol{\lambda}, \boldsymbol{\lambda}^u, \boldsymbol{\lambda}^e, \mu, \boldsymbol{\mu}^h, \boldsymbol{\mu}^r) \\ &= -D + \sum_{i\in I} \lambda_i (D - t_i^{cb} \frac{B}{C} \log_2(1 + \frac{p_i^{cb} h_i^{cb}}{N_0})) \\ &+ \sum_{i\in I} \lambda_i^u (D - t_i^{ucb} R_i^u) + \sum_{i\in I} \lambda_i^e (p_i^{cb} t_i^{cb} - \eta h_i^{cb} p_i^e t_i^e) \\ &+ \mu (\sum_{i\in I} t_i^h - T + T^{fly}) + \sum_{i\in I} \mu_i^h (t_i^r + t_i^e - t_i^h) \\ &+ \sum_{i\in I} \mu_i^r (t_i^{cb} + t_i^{ucb} - t_i^r). \end{aligned} \tag{28}$$

We refer to $\{\boldsymbol{\lambda}^*, \boldsymbol{\lambda}^{u*}, \boldsymbol{\lambda}^{e*}, \mu^*, \boldsymbol{\mu}^{h*}, \boldsymbol{\mu}^{r*}\}$ as the optimal Lagrange multipilers, and $\{D^*, \boldsymbol{p}^{cb*}, \boldsymbol{t}^{b*}\}$ as the optimal variables. By using the Karush-Kuhn-Tucker (KKT) conditions, we set the first-order derivatives of Lagrange function L with respect to optimal variables to zero. Thus we have

$$\sum_{i\in I} \lambda_i^* + \sum_{i\in I} \lambda_i^{u*} = 1 \tag{29}$$

$$\lambda_i^{e*}(p_i^{cb*} + p_i^{ee}) = \lambda_i^* \frac{B}{C} \log_2(1 + \frac{p_i^{cb*} h_i^{cb}}{N_0}), \quad \forall i \in I, \tag{30}$$

$$\mu^{r*} = \lambda_i^{u*} R_i^u, \quad \forall i \in I, \tag{31}$$

$$\mu^* = \mu_i^{h*}, \quad \forall i \in I, \tag{32}$$

$$\mu^{h*} = \mu_i^{r*}, \quad \forall i \in I, \tag{33}$$

$$\mu^{h*} = \lambda_i^{e*} p_i^{ee}, \quad \forall i \in I, \tag{34}$$

$$\lambda_i^{e*} = \lambda_i^* \frac{B}{C} \frac{h_i^{cb}}{\ln 2}, \quad \forall i \in I, \tag{35}$$

where $p_i^{ee} = p_i^e \eta h_i^{cb}$ is the received WPT power of the BIoTD.

Lemma 3. $\mu^* \neq 0$.

Proof. Reductio ad absurdum method is applied to demonstrate **Lemma 3**.

Assuming $\mu^* = 0$, by considering (30)-(35), we can get that $\mu^* = \mu_i^{h*} = \mu_i^{r*} = \lambda_i^* = \lambda_i^{u*} = \lambda_i^{e*} = 0, \forall i$, which is contradictory with (29), *i.e*, $\mu^* \neq 0$. ■

According to (30)-(35) and **Lemma 3**, we can find that all of the Lagrange multipliers are not equal to zero. Furthermore, the complementary slackness condition indicates that all of the inequality constraints in **P3** are not active at the optimum. Thus, the inequality constraints in **P3** take the equal sign.

According to (30) and (35), we obtain

$$(\ln 2) \log_2(1 + \frac{p_i^{cb*} h_i^{cb}}{N_0})(\frac{N_0}{h_i^{cb}} + p_i^{cb*}) - p_i^{cb*} - p_i^{ee} = 0. \tag{36}$$

We regard the Left-Hand Side (LHS) of (36) as a function with respect to the transmit power p_i^{cb}, and the function is expressed as

$$\Phi_i(p_i^{cb}) \triangleq (\ln 2) \log_2(1 + \frac{p_i^{cb} h_i^{cb}}{N_0})(\frac{N_0}{h_i^{cb}} + p_i^{cb}) - p_i^{cb} - p_i^{ee}, \tag{37}$$

and the optimal transmit power p_i^{cb*} is the zero of the function $\Phi_i(p_i^{cb})$.

The derivative of (37) is $\Phi_i^{'}(p_i^{cb}) = (\ln 2) \log_2(1 + \frac{p_i^{cb} h_i^{cb}}{N_0})$, which is always positive due to $p_i^{cb} > 0$. Therefore, we can conclude that $\Phi_i(p_i^{cb})$ is monotonically increasing with respect to p_i^{cb}. When $p_i^{cb} = 0$, the function value is $\Phi_i(0) = -p_i^{ee}$ which is less than zero, and

$$\lim_{p_i^{cb} \to +\infty} \Phi_i(p_i^{cb}) = +\infty. \tag{38}$$

Thus, the function $\Phi_i(p_i^{cb})$ must have a positive zero point p_i^{cb*} which can be obtained by a binary-search method.

After acquiring the p_i^{cb*}, we can get the other optimal values by solving the equations consisting of the constraints of **P3** for which the equal sign holds. The solutions are

$$\begin{aligned} &D^* = \frac{T - T^{fly}}{\sum_{i\in I} (\frac{p_i^{cb*}}{p_i^{ee} R_i^{cb*}} + \frac{1}{R_i^{cb*}} + \frac{1}{R_i^u})}, \\ &t_i^{cb*} = \frac{D^*}{R_i^{cb*}}, \quad t_i^{ucb*} = \frac{D^*}{R_i^u}, \quad t_i^{e*} = \frac{p^{cb*} t^{cb*}}{p_i^{ee}}, \quad \forall i \in I, \\ &t_i^{r*} = t_i^{cb*} + t_i^{ucb*}, \quad t_i^{h*} = t_i^{e*} + t_i^{r*}, \quad \forall i \in I. \end{aligned} \tag{39}$$

where $R_i^{cb*} = \frac{B}{C} \log_2(1 + \frac{p_i^{cb*} h_i^{cb}}{N_0})$.

D. Hovering positions Optimization

Given the link schedule $\boldsymbol{\alpha}$, the transmit power $\boldsymbol{p}^c$, and the UAV hovering time $\boldsymbol{t}^h$, the problem **P1** is simplified as

$$\begin{aligned} (\mathbf{P4}): &\max_{\boldsymbol{U}, D, \boldsymbol{t}^c, \boldsymbol{t}^{uc}, \boldsymbol{t}^r, \boldsymbol{t}^e} \quad D \\ &s.t. \quad (17a) - (17c), (17e), (17f), (17j). \end{aligned} \tag{40}$$

It is necessary to mention that the $\boldsymbol{U}$ is optimized cooperatively with the time variables $\boldsymbol{t}^c, \boldsymbol{t}^{uc}, \boldsymbol{t}^r, \boldsymbol{t}^e$, while the variable $\boldsymbol{t}^h$ is fixed.

1) Problem Form Simplification: The range of a specific hovering point $\boldsymbol{u}_i$ is a straight-line segment, which is marked as $L_i, \forall i \in I$. For the k-th IoTD in N_i^c, we define the distance from the k-th IoTD to the line segment L_i as $\sqrt{H_{i,k}}$, and the $\boldsymbol{w}_{i,k}^c$ component which is in the same dimensionality with u_i as $g_{i,k}$. Thus, the distance from the k-th IoTD in N_i^c to $\boldsymbol{u}_i$ can be re-expressed by

$$d_{i,k}^c(u_i) = \sqrt{(u_i - g_{i,k})^2 + H_{i,k}}, \quad \forall k \in N_i^c, \forall i \in I. \tag{41}$$

Similarly, the distance from the L_i to the related AP is H_i^u, and the related AP's coordinate component that is in the same dimensionality with $\boldsymbol{u}_i$ is g_i^u. Thus, the d_i^u is re-expressed as

$$d_i^u(u_i) = \sqrt{(u_i - g_i^u)^2 + H_i^u}, \quad \forall i \in I. \tag{42}$$

Inspired by the last two sub-problems, finding the BIoTD is the key to solving the problem. But unlike the problem **P2**, in **P4**, the BIoTD cannot be found directly because of the indetermination of the u_i. Therefore, we derived a two layers method for finding a suboptimal solution of the problem **P4**. The first layer (*i.e.*, the iteration layer) is to iterate each IoTD and regards it as the BIoTD to obtain an simplified problem. In the second layer, we solve the simplified problem by a bisection method.

For the k-th IoTD in N_i^c, we firstly assume it as the BIoTD at $\boldsymbol{u}_i$, and only the assumptive BIoTD is considered. Meanwhile, due to the UAV hovering time t_i^h at each hovering point is given, **P4** can be split into four uncoupled subproblems. Therefore, the problem only with respect to one hovering position $\boldsymbol{u}_i$ and one IoTD $\boldsymbol{w}_{i,k}^c$ is formulated:

$$(\mathbf{P5}): \min_{t_{i,k}^c, t_{i,k}^{uc}, t_i^r, t_i^e, u_i, D_{i,k}} \quad -D_{i,k} \tag{43}$$

$$s.t. \quad D_{i,k} - t_{i,k}^c R_{i,k}^c(u_i) \le 0, \tag{43a}$$

$$D_{i,k} - t_{i,k}^{uc} R_i^u(u_i) \le 0, \tag{43b}$$

$$p_{i,k}^c t_{i,k}^c - \frac{\eta h_0 p_i^e t_i^e}{(u_i - g_{i,k})^2 + H_{i,k}} \le 0, \tag{43c}$$

$$t_i^r + t_i^e \le t_i^h, \tag{43d}$$

$$t_{i,k}^c + t_{i,k}^{uc} \le t_i^r, \tag{43e}$$

$$0 \le u_i \le u_i^{max}, \tag{43f}$$

where $D_{i,k}$ is the data volume of the assumptive BIoTD, $R_{i,k}^c(u_i) = \log_2(1 + \frac{p_{i,k}^c h_0}{N_0 (d_{i,k}^c(u_i))^2})$ and $R_i^u(u_i) = \log_2(1 + \frac{p_i^u h_0}{N_0 (d_i^u(u_i))^2})$ are the data rate of the BIoTD-UAV channel and the UAV-AP channel, respectively. The unit of $D_{i,k}$ is bit/Hz, and the unit of $R_{i,k}^c(u_i)$ and $R_i^u(u_i)$ is bit/s/Hz.

2) Iteration Layer: Supposing the optimal u_i of **P5** is u_i^k. To solve the problem **P4**, we initiate an empty set U_i^a that contains the candidate solution of u_i and put all the $u_i^k, \forall k \in N_i^c$ into the U_i^a.

Besides, we define the

$$k^{next} = \arg\max_{j \in N_i^c} \quad (u_i^k - g_{i,j})^2 + H_{i,j}, \tag{44}$$

which is the index of the farthest IoTD in N_i^c when $u_i = u_i^k$. For the k-th and the j-th IoTD in N_i^c, if $k^{next} = j$ and $j^{next} = k$, which means they have the potentiality to simultaneously be the BIoTDs at the hovering position $\boldsymbol{u}_i$, then we obtain the position u_i^{kj} at which the UAV has the same distance with the k-th IoTD and the j-th IoTD as

$$u_i^{kj} = \frac{g_{i,k}^2 - g_{i,j}^2 + H_{i,k}^2 - H_{i,j}^2}{2(g_{i,k} - g_{i,j})}. \tag{45}$$

The u_i^{kj} is also put into the U_i^a. The next step is to calculate the achievable optimal value of the minimal data volume $D_{i,m}^a$ at each $u_{i,m}^a \in U_i^a$, where m is the index of the $u_{i,m}^a$ in U_i^a.

In order to calculate the optimal data volume $D_{i,m}^a$ for each $u_{i,m}^a$, we firstly find the true BIoTD $b_{i,m}^a \in N_i^c$ when $u_i = u_{i,m}^a$. We consider a special case of the problem **P5** when u_i is given as $u_{i,m}^a$ and the k is given as $b_{i,m}^a$. Then the **P5** becomes a linear programming problem which is readily to be solved by Lagrange method. The optimal data volume is

$$D_{i,m}^a = \frac{R_{i,m}^b t_i^h}{1 + \frac{R_{i,m}^b}{R_{i,m}^{ub}} + \frac{p_{i,m}^{cb}}{p_{i,m}^{eeb}}}, \tag{46}$$

where $R_{i,m}^b, R_{i,m}^{ub}$ are respectively the IoTD-UAV and the UAV-AP channel rate ralated to the IoTD $b_{i,m}^a$ when $u_i = u_{i,m}^a$, $p_{i,m}^{cb}$ is the transmit power of the IoTD $b_{i,m}^a$, and $p_{i,m}^{eeb}$ is the received WPT power of the IoTD $b_{i,m}^a$. Finally, we get the optimal index of candidates in the set U_i^a with

$$m^* = \arg \max_{m \in \{1,2,\ldots,|U_i^a|\}} D_{i,m}^a. \tag{47}$$

If u_{i,m^*}^a is in the range of $[0, u_i^{max}]$, then it is the solution of the UAV hovering position in our derived heuristic method, i.e, the u_i^*. If $u_{i,m^*}^a > u_i^{max}$, we get that $u_i^* = u_i^{max}$, and if $u_{i,m^*}^a < 0$, we set $u_i^* = 0$.

*3) Solve **P5**:* The constraint (43f) is not considered at first, and the Lagrange multipliers associated with the constraints (43a)-(43e) are λ, μ, ω_1, ω_2 and ω_3, respectively. Hence, the Lagrange duel function of **P5** is

$$\begin{aligned} &L(D_{i,k}, t_{i,k}^c, t_{i,k}^{uc}, t_i^r, t_i^e, u_i, \lambda, \mu, \omega_1, \omega_2, \omega_3) \\ &= -D_{i,k} + \lambda(D_{i,k} - t_{i,k}^c R_{i,k}^c(u_i)) \\ &+ \mu(D_{i,k} - t_{i,k}^{uc} R_i^u(u_i)) + \omega_1(p_{i,k}^c t_{i,k}^c - \frac{\eta h_0 p_i^e t_i^e}{(u_i - g_{i,k})^2 + H_{i,k}}) \\ &+ \omega_2(t_r^i + t_i^e - t_i^h) + \omega_3(t_{i,k}^c + t_{i,k}^{uc} - t_i^r). \end{aligned} \tag{48}$$

We use $\{t_{i,k}^{ck}, t_{i,k}^{uck}, t_i^{rk}, t_i^{ek}, u_i^k, D_{i,k}^k, \lambda^k, \mu^k, \omega_1^k, \omega_2^k, \omega_3^k\}$ to represent the optimal solutions and the optimal Lagrange multipliers. By employing the KKT conditions, we have

$$\lambda^k + \mu^k = 1, \tag{49}$$

$$\omega_1^k + \omega_3^k = \lambda^k R_{i,k}^c(u_i^k), \tag{50}$$

$$\omega_3^k = \mu^k R_i^u(u_i^k), \tag{51}$$

$$\omega_2^k = \omega_1^k \frac{A^e}{(u_i^k - g_{i,k})^2 + H_{i,k}}, \tag{52}$$

$$\omega_2^k = \omega_3^k, \tag{53}$$

$$\frac{2\lambda^k t_{i,k}^{ck} A}{\ln 2} \phi_1(u_i^k) + \frac{2\mu^k t_{i,k}^{uck} A^u}{\ln 2} \phi_2(u_i^k) + 2\omega_1^k t_i^{ek} B \phi_3(u_i^k) = 0, \tag{54}$$

where

$$A = \frac{p_{i,k}^c h_0}{N_0}, \quad A^u = \frac{p_i^u h_0}{N_0}, \quad A^e = \frac{p_i^e \eta h_0}{p_{i,k}^c},$$

$$\phi_1(u_i) = \frac{u_i - g_{i,k}}{((u_i - g_{i,k})^2 + H_{i,k})^2 + A((u_i - g_{i,k})^2 + H_{i,k})},$$

$$\phi_2(u_i) = \frac{u_i - g_i^u}{((u_i - g_i^u)^2 + H_i^u)^2 + A^u((u_i - g_i^u)^2 + H_i^u)},$$

$$\phi_3(u_i) = \frac{u_i - g_{i,k}}{((u_i - g_{i,k})^2 + H_{i,k})^2}.$$

Similar to **Lemma 3**, it is easy to get that all of the Lagrange multipliers are not zero due to the equation (49). According to the complementary slackness condition, the following equalities hold:

$$D_{i,k}^k - t_{i,k}^{ck} R_{i,k}^c(u_i^k) = 0, \tag{55}$$

$$D_{i,k}^k - t_{i,k}^{uck} R_i^u(u_i^k) = 0, \tag{56}$$

$$p_{i,k}^c t_{i,k}^{ck} - \frac{\eta h_0 p_i^e t_i^{ek}}{(u_i^k - g_{i,k})^2 + H_{i,k}} = 0, \tag{57}$$

$$t_i^{rk} + t_i^{ek} = t_i^h, \tag{58}$$

$$t_{i,k}^{ck} + t_{i,k}^{uck} = t_i^{rk}. \tag{59}$$

From (55)-(57) and (50)-(53), we define

$$c_1(u_i^k) = \frac{t_{i,k}^{ck}}{t_{i,k}^{uck}} = \frac{R_{i,k}^c(u_i^k)}{R_i^u(u_i^k)}, \tag{60}$$

$$c_2(u_i^k) = \frac{t_{i,k}^{ck}}{t_i^{ek}} = \frac{A^e}{(u_i^k - g_{i,k})^2 + H_{i,k}}, \tag{61}$$

$$\theta_1(u_i^k) = \frac{\omega_1^k}{\omega_2^k} = \frac{(u_i^k - g_{i,k})^2 + H_{i,k}}{A^e}, \tag{62}$$

$$\theta_2(u_i^k) = \frac{\lambda^k}{\omega_2^k} = \frac{1 + \theta_1(u_i^k)}{R_{i,k}^c(u_i^k)}, \tag{63}$$

$$\theta_3(u_i^k) = \frac{\mu^k}{\omega_2^k} = \frac{1}{R_i^u(u_i^k)}. \tag{64}$$

Thus, from (58), (59), (49) and (60)-(64) we have

$$t_{i,k}^{ck} = \frac{t_i^h}{1 + c_1 + c_2}, t_{i,k}^{uck} = \frac{c_1 t_i^h}{1 + c_1 + c_2}, t_i^{ek} = \frac{c_2 t_i^h}{1 + c_1 + c_2}, \tag{65}$$

$$\omega_2^k = \frac{1}{\theta_2 + \theta_3}, \lambda^k = \frac{\theta_2}{\theta_2 + \theta_3}, \mu^k = \frac{\theta_3}{\theta_2 + \theta_3}, \omega_1^k = \frac{\theta_1}{\theta_2 + \theta_3}. \tag{66}$$

To figure out the u_i^k, we plug (65) and (66) into the equation (54), then the equation about u_i^k holds:

$$\theta_2 A \phi_1 + \theta_3 c_1 A^u \phi_2 + \theta_1 c_2 A^e \phi_3 \ln 2 = 0. \tag{67}$$

The LHS of (67) can be regard as a function $G(u_i)$ with respect to u_i, and the optimal solution u_i^k is the zero point of the function where

$$\begin{aligned} G(u_i) = & \frac{(u_i - g_{i,k})^2 + H_{i,k} + A^e}{A^e \log_2(1 + \frac{A}{(u_i - g_{i,k})^2 + H_{i,k}})} \\ & \times \frac{A(u_i - g_{i,k})}{((u_i - g_{i,k})^2 + H_{i,k})^2 + A((u_i - g_{i,k})^2 + H_{i,k})} \\ & + \frac{1}{\log_2(1 + \frac{A}{(u_i - g_{i,k})^2 + H_{i,k}})} \\ & \times \frac{A^u(u_i - g_i^u)}{((u_i - g_i^u)^2 + H_i^u)^2 + A^u((u_i - g_i^u)^2 + H_i^u)} \\ & + \frac{A^e(u_i - g_{i,k})}{((u_i - g_{i,k})^2 + H_{i,k})^2} \ln 2. \end{aligned} \tag{68}$$

We use g^{max} to represent $\max\{g_{i,k}, g_i^u\}$ and g^{min} to express $\min\{g_{i,k}, g_i^u\}$. It is obvious that when $u_i > g^{max}$, the function value of $G(u_i)$ is always positive, and if $u_i < g^{min}$, we have $G(u_i) < 0$. Thus, the zero point u_i^k falls within the range (g^{min}, g^{max}). We introduce a variable x to replace the $u_i - g_{i,k}$ in (68), and the equation $G(u_i) = G(x + g_{i,k}) = 0$ can be re-expressed by $P(x) = 0$, where

$$\begin{aligned} P(x) = & \frac{A}{A^e} \frac{x^3 + (H_{i,k} + A^e)x}{x^2 + H_{i,k} + A} \\ & + \frac{A^u(x + \Delta)(x^2 + H_{i,k})}{((x + \Delta)^2 + H_i^u)^2 + A^u((x + \Delta)^2 + H_i^u)} \\ & + \frac{A^e x}{x^2 + H_{i,k}} \log_2(1 + \frac{A}{x^2 + H_{i,k}}) \ln 2, \end{aligned} \tag{69}$$

in which $\Delta = g_{i,k} - g_i^u \in \mathbb{R}$ is the difference of $g_{i,k}$ and g_i^u. When $\Delta > 0$, which means $g_{i,k} > g_i^u$, the proposition that the variable u_i is in the range $(g^{min}, g^{max}) = (g_i^u, g_{i,k}) = (g_{i,k} - \Delta, g_{i,k})$ is equivalent to the proposition that the variable x is in $(-\Delta, 0)$. Similarly, when $\Delta < 0$, $u_i \in (g^{min}, g^{max})$ is equivalent to $x \in (0, -\Delta)$. When $x = 0$, the value $P(0)$ equals $\frac{A^u H_{i,k} \Delta}{(\Delta^2 + H_i^u)^2 + A^u(\Delta^2 + H_i^u)}$, which has the same sign with Δ. When $x = -\Delta$, the function value

$$\begin{aligned} P(-\Delta) = & \frac{A}{A^e} \frac{(-\Delta)^3 + (H_{i,k} + A^e)(-\Delta)}{\Delta^2 + H_{i,k} + A} \\ & + \frac{A^e(-\Delta)}{\Delta^2 + H_{i,k}} \log_2(1 + \frac{A}{\Delta^2 + H_{i,k}}) \ln 2, \end{aligned} \tag{70}$$

has a different sign with Δ. As we can see, the function $P(x)$ is a continuous function with respect to x, and the function $P(x)$ change a sign at the endpoints of the interval $[0, -\Delta]$ or $[-\Delta, 0]$, which means the function $P(x)$ has at least one zero x^* between 0 and $-\Delta$, and we can obtain one zero by the binary search algorithm. It has to be mentioned that the monotonicity of $P(x)$ is hard to discuss, and we cannot prove that the $P(x)$ is a monotonic function with respect to x. Therefore, there may be more than one zero of $P(x)$. But we only need to get one zero of $P(x)$ as the suboptimal solution and the binary search algorithm can ensure that we can get at least a legal zero. The performance of the obtained suboptimal solution of the UAV's hovering points is evaluated at the subsection V-D2.

Thus, the optimal u_i^k of the problem **P5** can be obtained by $u_i^k = x^* + g_{i,k}$. The procedures to optimize UAV hovering points is summarized in **Algorithm 2**.

E. Overall Algorithm and Analysis

The BCD-based algorithm for solving the problem **P1** is given in **Algorithm 3**. The initial UAV hovering position $\boldsymbol{U}^{(0)}$ can be randomly selected within the feasible region. We introduce an iterative number k and the maximal iterative times k^{max}. Given $\boldsymbol{U}^{(k-1)}$, the link schedule $\boldsymbol{\alpha}^{(k)}$ can be solved by performing **Algorithm 1**. Then, we obtain the power and time variables $\boldsymbol{p}^{c(k)}$, $\boldsymbol{t}^{(k)}$, and the achievable minimal data volume of the system $D^{(k)}$ under the given $\boldsymbol{\alpha}^{(k)}$ and $\boldsymbol{U}^{(k-1)}$ by solving the **P2**. If we get a value $D^{(k)}$ which is better than the historical best value $best$, we update the best solution recorder. Before the next iteration, we update the $\boldsymbol{U}^{(k-1)}$ to $\boldsymbol{U}^{(k)}$ by **Algorithm 2**.

Algorithm 2 Algorithm for Optimizing UAV hovering points

Input: $\boldsymbol{\alpha}$, $\boldsymbol{p}^c$, $\boldsymbol{t}^h$
Output: $\boldsymbol{U}^*$

for $i \in I$ **do**
  for $k \in N_i^c$ **do**
    Obtain u_i^k by solving **P5**;
    Put u_i^k into the set U_i^a;
    Obtain k^{next} by (44);
    $\boldsymbol{next}(k) \leftarrow k^{next}$;
  end for
  for $k \in N_i^c$ **do**
    if $\boldsymbol{next}(k) \neq k$ and $\boldsymbol{next}(\boldsymbol{next}(k)) = k$ **then**
      $j \leftarrow \boldsymbol{next}(k)$
      Obatin u_i^{kj} by (45) and put u_i^{kj} into the set U_i^a;
    end if
  end for
  for $u_{i,m}^a \in U_i^a$ **do**
    Obtain $D_{i,m}^a$ by (46);
    $\boldsymbol{ach}(m) \leftarrow D_{i,m}^a$;
  end for
  $m^* \leftarrow \arg\max_m \boldsymbol{ach}$;
  $u_i^* \leftarrow u_{i,m^*}^a$;
end for
return $\boldsymbol{U}^* = \{u_i^*\}$;

Algorithm 3 Overall Algorithm

Input: initial hovering positions $\boldsymbol{U}^{(0)}$
Output: $\boldsymbol{\alpha}^*$, $\boldsymbol{U}^*$, $\boldsymbol{p}^{c*}$, $\boldsymbol{t}^*$, D^*

$k \leftarrow 1$, $best \leftarrow 0$;
while $k < k^{max}$ **do**
  Obatin $\boldsymbol{\alpha}^{(k)}$ by **Algorithm 1**;
  Obtain $\boldsymbol{p}^{c(k)}$, $\boldsymbol{t}^{(k)}$, $D^{(k)}$ by solving **P2**;
  if $D^{(k)} > best$ **then**
    $best \leftarrow D^{(k)}$;
    $\boldsymbol{\alpha}^* \leftarrow \boldsymbol{\alpha}^{(k-1)}$, $\boldsymbol{U}^* \leftarrow \boldsymbol{U}^{(k)}$, $\boldsymbol{p}^{c*} \leftarrow \boldsymbol{p}^{c(k)}$, $\boldsymbol{t}^* \leftarrow \boldsymbol{t}^{(k)}$;
  end if
  Obtain $\boldsymbol{U}^{(k)}$ by **Algorithm 2**;
  $k \leftarrow k + 1$;
end while
return $\boldsymbol{\alpha}^*$, $\boldsymbol{U}^*$, $\boldsymbol{p}^{c*}$, $\boldsymbol{t}^*$, $D^* \leftarrow best$;

The iterative **Algorithm 3** always converges. The proof is established by showing that the minimum throughput of the system is non-decreasing when the sequence $(\boldsymbol{\alpha}, \boldsymbol{p}, \boldsymbol{t}, \boldsymbol{U})$ is updated.

The complexity of **Algorithm 3** in each iteration lies in its sub-problems. For **Algorithm 1**, the complexity is $\mathcal{O}(n_0^2)$. The complexity of performing the second subproblem is $\mathcal{O}(N + L_1)$, where L_1 is the iteration numbers for finding the zero point of (37) by binary-search method. As for the **Algorithm 2**, the computational complexity is $\mathcal{O}(N^2 + NL_2)$, where L_2 is the searching numbers for solving the zero point of function (69). Therefore, the total complexity of **Algorithm 3** is $\mathcal{O}(L_3(N^2 + L_1 + NL_2))$ in which L_3 is the iteration number of the **Algorithm 3**.

F. Discussion on Heterogeneous IoTDs

The above system model is based on the assumption that the IoTDs are homogenous(*i.e.*, their data rate requirements are similar). However, in a real building SHM scenario, different types of IoTDs often have different base rate requirements, which means they are heterogeneous. In order to improve the generalizability of this paper, we propose a method to deal with the heterogeneous devices problem.

We first define the baseline throughput requirements $\Gamma_{i,k}$ for each device, respectively, and define a unit throughput γ (*e.g.* 500kbps). Moreover, all rate requirements are integral multiples of the unit throughput. For instance, the requirement of an IoTD is $\Gamma_{i,k} = n\gamma$, where $n \in \mathbb{Z}^+$. Then, we regarded this IoTD as n Virtual IoTDs (VIoTD). For a real IoTD, the respective VIoTDs have the same throughput requirement γ and the same position. By treating all heterogeneous IoTDs as homogenous VIoTDs, the problem becomes solvable by the algorithm proposed in this paper.

Specifically, for a real side IoTD, the respective VIoTDs can only connect to a specific hover point. The proposed algorithm can guarantee that these VIoTDs have the same optimal power $p_{i,k}^c$ and optimal time $t_{i,k}^c, t_{i,k}^{uc}$ values, respectively. The real IoTDs uses n times the bandwidth allocated to each VIoTD, (*i.e.* $n \times B/C$), to achieve n times throughput of one VIoTD.

For a real IoTD on the top plane, the respective VIoTDs may link to different hovering points. For example, if 2 VIoTDs link to $\boldsymbol{u}_1$ and 3 VIoTDs link to $\boldsymbol{u}_2$, the real IoTD will use the bandwidth $\frac{2B}{C}$ to connect with $\boldsymbol{u}_1$ and use the bandwidth $\frac{3B}{C}$ to communicate with the UAV hovering at $\boldsymbol{u}_2$.

G. Discussion on Low-floor IoTDs

Depending on the location, the side IoTDs can be divided into the high-floor and low-floor IoTDs. High-floor IoTDs require forwarding services of the UAV. But for low-floor IoTDs, they can communicate directly with the AP because of the short distance from the AP. Therefore, in our model and algorithm presented above, only high-floor IoTDs are considered.

The division of the side IoTDs varies with the problem parameters. Therefore, we propose a method to classify side devices dynamically.

Firstly, all the side IoTDs are treated as high-floor IoTDs. Secondly, we update the UAV's hovering positions by **Algorithm 3**. Thirdly, among the existing high-floor IoTDs, we treat the devices closer to the AP than to the UAV as low-floor IoTDs. Finally, we repeat the second and the third steps until the division case converges.

It is worth emphasizing that our later comparison algorithms are based on the same division of side IoTDs.

V. Numerical Results

In this section, numerical results are presented to validate the performance of our proposed algorithm with other benchmark schemes. The numerical results are obtained by MATLAB R2020a with an Intel i5-1135G7 2.4GHz CPU and 16GB RAM.

A. Setting

We consider a scenario where the IoTDs are randomly distributed on the surface of the building. The parameters in the simulation are summarized in TABLE II [28]–[30]. To reduce the influence of the random distribution, we independently repeated the experiments 10 times in Fig. 4 - 7, and the error bars in these figures represent the stand deviation.

TABLE II
SIMULATION PARAMETERS

Notation	Value	Notation	Value
L, W, H	40, 10, 40m	N_0	-60dBm
H_u	5m	η	0.8
r_u	5m	C	20
N	70	B	400MHz
n_i	10,15,15,15,15	v	10m/s
$\boldsymbol{\omega}_1^{ap}$	$(50m, -10m, 0)$	a	5m/s^2
$\boldsymbol{\omega}_2^{ap}$	$(-10m, 20m, 0)$	p^u, p^e	1, 10W
h_0	-20dB	T	240s

B. Convergence Performance

Firstly, we discuss the convergence performance of our proposed **Algorithm 3**. The optimal value versus the number of iterations is depicted in Fig. 3. From this figure, we can observe that the convergence curve is increasing with iterations, and the convergence speed is fast.

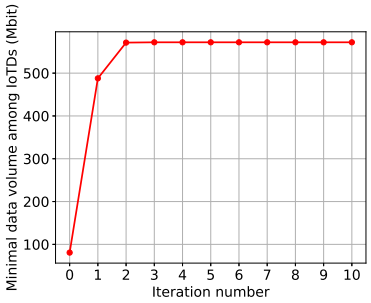

Fig. 3. Convergence behavior of the proposed **Algorithm 3**.

C. Algorithm Comparison

In this part, we compare our solution with other state-of-the-art approaches. For comparison purposes, our proposed algorithm is labeled as *BAHA* (*i.e.* the Bottleneck-Awared Heuristic Algorithm). The comparison algorithms are shown below:

1). **Game Theory(GT)** [31], [32]: The players of the game are all IoTDs and the UAV hovering points.

On the one hand, for each hovering position, we maximize the minimal throughput among linked IoTDs through one-dimensional exhaustive searching for the optimal hovering position. On the other hand, for each IoTD, we maximize its throughput by optimizing the power $\boldsymbol{p}^c$, time $\boldsymbol{t}$ and the link selection variable $\boldsymbol{\alpha}$. In detail, the power and time variables are optimized by Lagrange method, and the link selection is determined by proximity principle, respectively. After iterating through all IoTDs once, we regard the maximum WPT time among the IoTDs linked to the same hovering point as the WPT time for these IoTDs. Correspondingly, the other time variables are scaled down to meet (17e).

The GT method keeps repeating the above optimization until the result converge. This scheme is labeled as *GT*.

2). **Monte-Carlo Method(MC)**: In the *MC* scheme, we sample the solutions of **P1** randomly in large numbers and select the solution with the maximum objective function value as the algorithm solution.

During each sampling, we randomly construct a feasible solution exclude the variable D. Specifically, the constructing order is "$\boldsymbol{U}, \boldsymbol{\alpha}, \boldsymbol{p}^c, \boldsymbol{t}^h, \boldsymbol{t}^e, \boldsymbol{t}^r, \boldsymbol{t}^{uc}, \boldsymbol{t}^c$", and the constructed value should meet the constraints of **P1**. Finally, the objective value D can determined by (17a) and (17b).

In our simulation, the label *MC4* is the MC method with 1×10^4 times of attempts, and the scheme *MC6* tries 1×10^6 times to reach the solution.

TABLE III
AVERAGE TIME CONSUMPTION (IN SECOND).

Figure	Scheme			
	BAHA	*GT*	*MC4*	*MC6*
Fig. 4	0.059	1.916	4.675	458.788
Fig. 5(a)	0.128	2.098	5.148	505.056
Fig. 5(b)	0.066	1.924	4.645	456.622
Fig. 5(c)	0.067	1.917	4.652	456.803
Fig. 5(d)	0.056	1.907	4.623	456.750

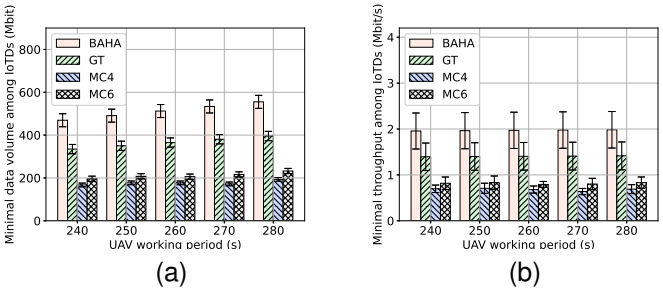

Fig. 4. Comparison versus working period. (a) minimal data volume among IoTDs versus the UAV working period. (b) minimal throughput among IoTDs versus the UAV working period.

Fig. 4 shows the minimal data volume and throughput among IoTDs versus the working period T under different schemes, and Table III illustrates the average time consumption of the *BAHA*, *GT*, *MC4* and *MC6* schemes.

As expected, from Fig. 4, the data volume increases with the working period T of the UAV, and the throughput is constant *w.r.t.* the period T. The reason is that the minimal throughput in our system is independent of the period T and the data volume is in linear correlation with the period T.

From Fig. 4, we can also observe that our proposed *BAHA* scheme outperforms the other benchmark algorithms. Meanwhile, the execution time of our proposed *BAHA* scheme is the shortest. The *MC6* scheme performs better than the *MC4* scheme due to more iterations. However, more attempts result in that the computation time of *MC6* is much longer than the *MC4* scheme's, which can be seen in TABLE III. Compared

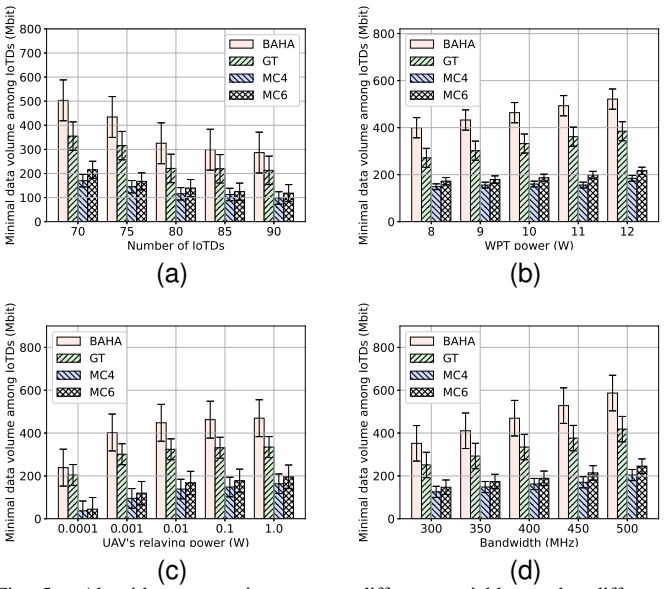

Fig. 5. Algorithm comparison versus different variables under different schemes in subsection V-C. (a) minimal data volume among IoTDs versus the total number of IoTDs. (b) minimal throughput among IoTDs versus the WPT power. (c) minimal throughput among IoTDs versus the UAV's relaying power. (d) minimal throughput among IoTDs versus the total communication bandwidth.

with *MC4*, the *GT* scheme takes less time to get a solution which has much better performance.

Fig. 5 demonstrates the relationship between data volume and the IoTD number, WPT power, UAV's relaying power, and channel bandwidth under different schemes, respectively. It can be seen from the Fig. 5(a) that the throughput decreases with the number of IoTDs, which is caused by the limited bandwidth resources. We utilize the OFDMA technology to eliminate communication interference between IoTDs, which means the greater the number of IoTDs, the less bandwidth is allocated for each IoTD. In Fig. 5(b), Fig. 5(c) and Fig. 5(d), we can see that the data volume increases with the WPT power, the UAV's relaying power and the channel bandwidth, respectively. When the WPT power increases, the IoTDs can harvest more energy for communication. Therefore, the transmit power and rate between the UAV and IoTDs can be larger, and the greater data volume can be achieved. When the UAV's relaying power increases, the UAV-AP channel can use less time to forward data. Thus, the time for the IoTDs to transmit data to UAV can be longer, and the data volume becomes greater. As for the bandwidth, with the increasing of bandwidth, the communication rate increases, which results in a larger amount of traffic.

From TABLE III, it can be seen that the time required for Fig. 5(a) is longer than that of other figures, because the average number of IoTDs in Fig. 5(a) is more, resulting in a larger problem scale and longer calculation time.

With regard to the performance of the algorithms involved in Fig. 5, our proposed *BAHA* has the most outstanding results, and the time consumed by our algorithm is the shortest in TABLE III. The contrast of performance and solving efficiency among the algorithms is similar to Fig. 4.

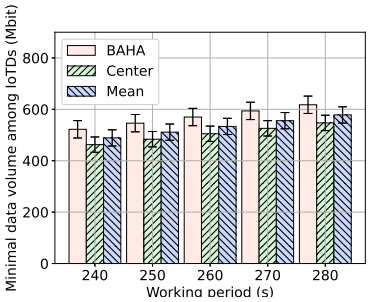

Fig. 6. Hovering strategies comparison.

D. Influence of Hovering Points

1) Comparison Between Different Hovering Strategies: Firstly, we evaluate our algorithm by comparing with different UAV's hovering strategies.

The benchmark hovering strategies are tagged with the *Center* and the *Mean* schemes. In the *Center* scheme, the UAV is hovering at the midpoint of each straight-line trajectory. While in the *Mean* strategy, for each straight line trajectory, the UAV is located at the projection of the centroid of all linked IoTD's locations on the trajectory. The variables except the hovering positions $\boldsymbol{U}$ are optimized by our proposed method.

The result is shown in Fig. 6. The data volume achieved by our proposed schemes are larger than the other hovering strategies, which means the proposed **Algorithm 2** can improve the system's minimal data volume. As the period T increases, the amount of data obtained increases linearly, as the data volume is in linear correlation with time.

2) Hovering Points Optimization Algorithm Comparison: For the sake of evaluating the performance of the **Algorithm 2**, we compare it with other schemes which replace **Algorithm 2** part of **Algorithm 3** with other state-of-art methods. The comparing algorithms are introduced below [33]:

1) **Particle Swarm Optimization (PSO)** [34]: PSO is a universal computational method that optimizes a problem by iteratively trying to improve a candidate solution with regard to a given measure of quality. The PSO method solves the problem by updating a population of candidate particles. In the PSO scheme, each particle is a four-dimensional vector which represents the hovering points $\boldsymbol{U}$. The fitness value of each particle is obtained by our algorithm for solving the other variables, (*i.e.* the **Algorithm 1** and the Lagrange method for optimizing $\boldsymbol{p}^c$ and $\boldsymbol{t}$), and the fitness value is the optimal data volume at the hovering points $\boldsymbol{U}$ represented by the particle. In this simulation, the number of particles in the swarm is 50, and the number of iterations is set as 100. This scheme is labeled as *PSO*.

2) **MC**: This scheme is labeled as *MCU*. The solution is obtained after massive random sampling the optimization variables within the feasible region. In this scheme, at each iteration, we randomly construct the hovering point variable $\boldsymbol{U}$ within the feasible region. Then our proposed methods for solving the other variables, (*i.e.* the **Algorithm 1** and the Lagrange method for optimizing $\boldsymbol{p}^c$ and $\boldsymbol{t}$) are successively used to obtain the optimal value. After a large number of attempts, the solution with the maximum optimal value among

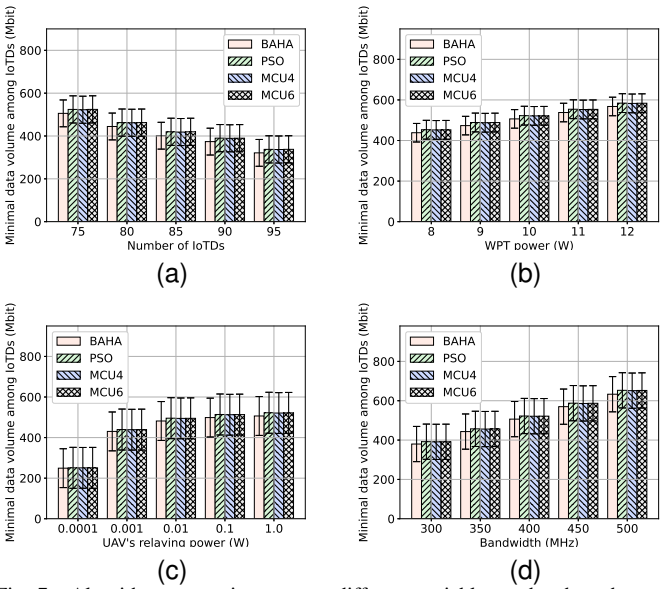

Fig. 7. Algorithm comparison versus different variables under the schemes in subsection V-D2. (a) minimal data volume among IoTDs versus the total number of IoTDs. (b) minimal throughput among IoTDs versus the WPT power. (c) minimal throughput among IoTDs versus the UAV's relaying power. (d) minimal throughput among IoTDs versus the total communication bandwidth.

all attempts will be assumed as the solution of the *MCU* scheme. Specifically, we take two different schemes which are named as *MCU4* and *MCU6*, respectively. The difference is that the sampling number of the *MCU4* scheme is 1×10^4, while the *MCU6* scheme's number of attempts is 1×10^6.

TABLE IV
AVERAGE TIME CONSUMPTION (IN SECOND).

Figure	Scheme			
	BAHA	*PSO*	*MCU4*	*MCU6*
Fig. 7(a)	0.130	3.248	6.348	623.881
Fig. 7(b)	0.053	2.960	5.767	572.503
Fig. 7(c)	0.062	2.989	5.712	568.241
Fig. 7(d)	0.059	3.022	5.712	569.172

Fig. 7 illustrates the data volume versus different comparison variables under the *BAHA*, *PSO* and *MCU* schemes. The trend of the data volume about the comparison variables in Fig. 7 is the same as that in Fig. 5.

Regarding the performance, we can see that the *PSO*, *MCU4* and *MCU6* schemes have nearly identical performance. The reason why *MCU6* does not obtain a better solution than *MCU4* is that the variable $\boldsymbol{U}$ has only 4 dimensions, and the attempt number 1×10^4 is big enough. This phenomenon indicates that the solutions obtained by the *MCU* and *PSO* schemes are almost the optimal solution with respect to $\boldsymbol{U}$. The solution obtained by our Lagrange method for solving $\boldsymbol{U}$ is slightly smaller than that of the other models. However, the efficiency of *BAHA* is much higher, which can be observed from TABLE IV, indicating that the time complexity of our algorithm is lower than the benchmark schemes.

VI. CONCLUSION

In this paper, we investigate a UAV-enabled WPCN which is deployed at the surface of a cuboid building, where a UAV is dispatched to provide forwarding services and WPT services for the IoTDs, and two APs are utilized as the MEC servers. In order to maximize the throughput of the system while considering fairness among IoTDs, we formulate a problem to maximize the minimal throughput among IoTDs. We design an efficient BCD-based algorithm to solve the problem with a low algorithmic complexity. In the proposed algorithm, we simplify the problem by finding bottleneck IoTDs to reduce the computational effort of the algorithm. Simulation results indicate that our algorithm can achieve a better solution within a much shorter time. In the future work, multiple UAVs can be used to provide real-time forwarding services. Moreover, the scenarios where the building has more a complex shape should be considered.

ACKNOWLEDGMENTS

This work is jointly supported by Natural Science Foundation of Hunan Province, China(Grant No. 2021JJ30736), Changsha Municipal Natural Science Foundation (Grant No.kq2014112).

REFERENCES

[1] C. Scuro et al., "Internet of Things (IoT) for masonry structural health monitoring (SHM): Overview and examples of innovative systems," Construction and Building Materials, vol. 290, pp. 123092, 2021.

[2] J. Hu, K. Yang, G. Wen and L. Hanzo, "Integrated Data and Energy Communication Network: A Comprehensive Survey," in IEEE Communications Surveys & Tutorials, vol. 20, no. 4, pp. 3169-3219, Fourthquarter 2018, doi: 10.1109/COMST.2018.2860778.

[3] H. Tang, Q. Wu, W. Chen, J. Wang and B. Li, "Mitigating the Doubly NearFar Effect in UAV-Enabled WPCN," in IEEE Transactions on Vehicular Technology, vol. 70, no. 8, pp. 8349-8354, Aug. 2021, doi: 10.1109/TVT.2021.3096540.

[4] C. Wang et al., "Covert Communication Assisted by UAV-IRS," in IEEE Transactions on Communications, 2022, doi: 10.1109/TCOMM.2022.3220903.

[5] X. Pang, M. Sheng, N. Zhao, J. Tang, D. Niyato and K. -K. Wong, "When UAV Meets IRS: Expanding Air-Ground Networks via Passive Reflection," in IEEE Wireless Communications, vol. 28, no. 5, pp. 164-170, October 2021, doi: 10.1109/MWC.010.2000528.

[6] H. Im et al., "Embedded Structural-Durability Health-Monitoring System Integrated With Multisensors and a Wideband Antenna," in IEEE Internet of Things Journal, vol. 9, no. 18, pp. 17480-17487, 15 Sept.15, 2022, doi: 10.1109/JIOT.2022.3156608.

[7] R. Misra, H. Jalali, P. Rizzo and S. J. Dickerson, "Wireless Node for Highly Nonlinear Solitary Wave Transducers," in IEEE Sensors Journal, vol. 22, no. 4, pp. 3540-3552, 15 Feb.15, 2022, doi: 10.1109/JSEN.2021.3136859.

[8] K. Yan, Y. Zhang, Y. Yan, C. Xu, S. Zhang, "Fault diagnosis method of sensors in building structural health monitoring system based on communication load optimization," Computer Communications, vol. 159, pp. 310-316, 2020.

[9] J. Baek, S. I. Han and Y. Han, "Optimal UAV Route in Wireless Charging Sensor Networks," in IEEE Internet of Things Journal, vol. 7, no. 2, pp. 1327-1335, Feb. 2020, doi: 10.1109/JIOT.2019.2954530.

[10] H. Hu, X. Zhou, Q. Wang and R. Q. Hu, "Online computation offloading and trajectory scheduling for UAV-enabled wireless powered mobile edge computing," in China Communications, vol. 19, no. 4, pp. 257-273, April 2022, doi: 10.23919/JCC.2022.04.019.

[11] X. Gu, G. Zhang, M. Wang, W. Duan, M. Wen and P. -H. Ho, "UAV-Aided Energy-Efficient Edge Computing Networks: Security Offloading Optimization," in IEEE Internet of Things Journal, vol. 9, no. 6, pp. 4245-4258, 15 March15, 2022, doi: 10.1109/JIOT.2021.3103391.

[12] Y. Du, K. Yang, K. Wang, G. Zhang, Y. Zhao and D. Chen, "Joint Resources and Workflow Scheduling in UAV-Enabled Wirelessly-Powered MEC for IoT Systems," in IEEE Transactions on Vehicular Technology, vol. 68, no. 10, pp. 10187-10200, Oct. 2019, doi: 10.1109/TVT.2019.2935877.

[13] Y. Liu, K. Xiong, Q. Ni, P. Fan and K. B. Letaief, "UAV-Assisted Wireless Powered Cooperative Mobile Edge Computing: Joint Offloading, CPU Control, and Trajectory Optimization," in IEEE Internet of Things Journal, vol. 7, no. 4, pp. 2777-2790, April 2020, doi: 10.1109/JIOT.2019.2958975.
[14] L. Xie, J. Xu and R. Zhang, "Throughput Maximization for UAV-Enabled Wireless Powered Communication Networks," in IEEE Internet of Things Journal, vol. 6, no. 2, pp. 1690-1703, April 2019, doi: 10.1109/JIOT.2018.2875446.
[15] L. Xie, J. Xu and Y. Zeng, "Common Throughput Maximization for UAV-Enabled Interference Channel With Wireless Powered Communications," in IEEE Transactions on Communications, vol. 68, no. 5, pp. 3197-3212, May 2020, doi: 10.1109/TCOMM.2020.2971488.
[16] J. Du, Z. Wang, Z. Fan and X. Wan, "Sum Rate Maximization for UAV-Enabled Wireless Powered NOMA Systems," 2020 IEEE/CIC International Conference on Communications in China (ICCC), 2020, pp. 753-757, doi: 10.1109/ICCC49849.2020.9238850.
[17] Y. Liu et al., "Joint Communication and Computation Resource Scheduling of a UAV-Assisted Mobile Edge Computing System for Platooning Vehicles," in IEEE Transactions on Intelligent Transportation Systems, doi: 10.1109/TITS.2021.3082539.
[18] W. Lu et al., "Trajectory and Resource Optimization in OFDM-Based UAV-Powered IoT Network," in IEEE Transactions on Green Communications and Networking, vol. 5, no. 3, pp. 1259-1270, Sept. 2021, doi: 10.1109/TGCN.2021.3085747.
[19] M. Jiang, Y. Li, Q. Zhang and J. Qin, "Joint Position and Time Allocation Optimization of UAV Enabled Time Allocation Optimization Networks," in IEEE Transactions on Communications, vol. 67, no. 5, pp. 3806-3816, May 2019, doi: 10.1109/TCOMM.2019.2896973.
[20] J. Wang, C. Jin, Q. Tang, N. N. Xiong and G. Srivastava, "Intelligent Ubiquitous Network Accessibility for Wireless-Powered MEC in UAV-Assisted B5G," in IEEE Transactions on Network Science and Engineering, vol. 8, no. 4, pp. 2801-2813, 1 Oct.-Dec. 2021, doi: 10.1109/TNSE.2020.3029048.
[21] Z. Wang, G. Zhang, Q. Wang, K. Wang and K. Yang, "Completion Time Minimization in Wireless-Powered UAV-Assisted Data Collection System," in IEEE Communications Letters, vol. 25, no. 6, pp. 1954-1958, June 2021, doi: 10.1109/LCOMM.2021.3057069.
[22] T. D. Ponnimbaduge Perera, S. Panic, D. N. K. Jayakody, P. Muthuchidambaranathan and J. Li, "A WPT-Enabled UAV-Assisted Condition Monitoring Scheme for Wireless Sensor Networks," in IEEE Transactions on Intelligent Transportation Systems, vol. 22, no. 8, pp. 5112-5126, Aug. 2021, doi: 10.1109/TITS.2020.3018493.
[23] K. Li, W. Ni, E. Tovar and A. Jamalipour, "Deep Q-Learning based Resource Management in UAV-assisted Wireless Powered IoT Networks," ICC 2020 - 2020 IEEE International Conference on Communications (ICC), 2020, pp. 1-6, doi: 10.1109/ICC40277.2020.9149282.
[24] Y. Yu, J. Tang, J. Huang, X. Zhang, D. K. C. So and K. -K. Wong, "Multi-Objective Optimization for UAV-Assisted Wireless Powered IoT Networks Based on Extended DDPG Algorithm," in IEEE Transactions on Communications, vol. 69, no. 9, pp. 6361-6374, Sept. 2021, doi: 10.1109/TCOMM.2021.3089476.
[25] Y. Hu, X. Yuan, J. Xu and A. Schmeink, "Optimal 1D Trajectory Design for UAV-Enabled Multiuser Wireless Power Transfer," in IEEE Transactions on Communications, vol. 67, no. 8, pp. 5674-5688, Aug. 2019, doi: 10.1109/TCOMM.2019.2911294.
[26] D. Lee, "A Linear Acceleration Control for Precise Trajectory Tracking Flights of a Quadrotor UAV Under High-wind Environments," International Journal of Aeronautical and Space Sciences, vol. 22, no. 4, pp. 898-910, 2021.
[27] Boyd, S., Vandenberghe, L., Faybusovich, L.. Convex optimization. IEEE Transactions on Automatic Control 2006;51(11):18591859. doi:10.1109/TAC.2006.884922.
[28] W. Lu et al., "Resource and Trajectory Optimization for Secure Communications in Dual Unmanned Aerial Vehicle Mobile Edge Computing Systems," in IEEE Transactions on Industrial Informatics, vol. 18, no. 4, pp. 2704-2713, April 2022, doi: 10.1109/TII.2021.3087726.
[29] J. Wang, K. Liu and J. Pan, "Online UAV-Mounted Edge Server Dispatching for Mobile-to-Mobile Edge Computing," in IEEE Internet of Things Journal, vol. 7, no. 2, pp. 1375-1386, Feb. 2020, doi: 10.1109/JIOT.2019.2954798.
[30] K. Wang, K. Yang and C. S. Magurawalage, "Joint Energy Minimization and Resource Allocation in C-RAN with Mobile Cloud," in IEEE Transactions on Cloud Computing, vol. 6, no. 3, pp. 760-770, 1 July-Sept. 2018, doi: 10.1109/TCC.2016.2522439.
[31] Z. Luo and A. Huang, "Joint Game Theory and Greedy Optimization Scheme of Computation Offloading for UAV-Aided Network," 2021 31st International Telecommunication Networks and Applications Conference (ITNAC), 2021, pp. 198-203, doi: 10.1109/ITNAC53136.2021.9652130.
[32] M. -A. Messous, S. -M. Senouci, H. Sedjelmaci and S. Cherkaoui, "A Game Theory Based Efficient Computation Offloading in an UAV Network," in IEEE Transactions on Vehicular Technology, vol. 68, no. 5, pp. 4964-4974, May 2019, doi: 10.1109/TVT.2019.2902318.
[33] Q. Tang, L. Liu, C. Jin, J. Wang, Z. Liao, Y Luo, Tang, "An UAV-assisted mobile edge computing offloading strategy for minimizing energy consumption," Computer Networks, vol. 207, pp. 108857, 2022.
[34] Marini, Federico and Walczak, Beata, "Particle swarm optimization (PSO). A tutorial," Chemometrics and Intelligent Laboratory Systems, vol. 149, pp. 153-165, 2015.

Qiang Tang received the B.E., M.S., and Ph.D. degrees in control science and engineering from the Huazhong University of Science and Technology, Wuhan, China, in 2005, 2007, and 2010, respectively. He is an academic visitor sponsored by CSC in University of Essex during 2016-2017. He is currently a Lecturer with the School of Computer and Communication Engineering, Changsha University of Science and Technology, Changsha, China. His research interests include wireless networks, mobile edge computing, and smart grid.

Yong Yang received the B.E. degree in mechanical design, manufacturing and automation from the Hunan Normal University, Changsha, China, in 2021. His current reserch interests include mobile edge computing and wireless communication network.

Lixin Liu received the B.E. degree in computer science and technology from the school of computer science, Southwest Petroleum University, Chengdu, China, in 2020. Her current reserch interests include wireless UAV communication and mobile edge computing.

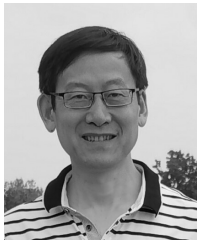

Kun Yang received his PhD from the Department of Electronic & Electrical Engineering of University College London (UCL), UK. He is currently a Chair Professor in the School of Computer Science & Electronic Engineering, University of Essex, leading the Network Convergence Laboratory (NCL), UK. He is also an affiliated professor at UESTC, China. Before joining in the University of Essex at 2003, he worked at UCL on several European Union (EU) research projects for several years. His main research interests include wireless networks and communications, IoT networking, data and energy integrated networks and mobile computing. He manages research projects funded by various sources such as UK EPSRC, EU FP7/H2020 and industries. He has published 400+ papers and filed 30 patents. He serves on the editorial boards of both IEEE (e.g., IEEE TNSE, IEEE ComMag, IEEE WCL) and non-IEEE journals (e.g., Deputy EiC of IET Smart Cities). He was an IEEE ComSoc Distinguished Lecturer (2020-2021). He is a Member of Academia Europaea (MAE), a Fellow of IEEE, a Fellow of IET and a Distinguished Member of ACM.